Available online at www.sciencedirect.com

ScienceDirect

Advances in Space Research 73 (2024) 3472–3485

ADVANCES IN SPACE RESEARCH (a COSPAR publication)

www.elsevier.com/locate/asr

Signature of thunderstorm induced acoustic and gravity waves at low latitude Indian sector

Soumen Datta *, Saurabh Das

Department of Astronomy, Astrophysics and Space Engineering, Indian Institute of Technology Indore, Indore, Madhya Pradesh 453552, India

Received 24 March 2023; received in revised form 1 September 2023; accepted 7 September 2023
Available online 12 September 2023

Abstract

This study reports thunderstorm-generated acoustic and gravity waves from a tropical location using newly launched Indian navigation system NavIC for the first time. The detection of acoustic wave components in travelling ionospheric disturbance (TID) measurement is very significant. In compared to acoustic wave gravity wave signature is more ubiquitous because gravity wave propagates in thermospheric altitude by dissipative filtering process. The turbulent nature in plasma characteristics due to strong vertical drift and plasma motion in lower latitude region generate strong scintillation effect and plasma bubble. Large temperature gradient at thermospheric altitude also provides a strong attenuation effect in this region for comparatively high frequency acoustic wave. We have found the TID signatures on TEC variation for acoustic wave up to 0.4 TECU for both the days whereas gravity wave induced signatures went up to 0.8 TECU. Measurements using GPS signal validate signatures obtained from the NavIC signal. The study shows the potential of application of NavIC system for middle atmosphere as well as thermospheric study and understanding of coupling process between various atmospheric layers in tropical region which is not well known so far.

Keywords: Thunderstorm; NavIC; Travelling ionospheric disturbance; Acoustic wave Gravity wave

1. Introduction

Research on the impact of different severe lower atmospheric phenomena and natural hazards such as cyclone, thunderstorm, volcanic eruption, earthquake etc. on various layer of ionosphere have been gaining high interest in recent past. Low frequency atmospheric waves which are major consequences of such natural hazards have been traced in various layers of the atmosphere. The atmospheric waves with period less than the acoustic cut-off period of the respective medium is known as acoustic wave. Acoustic waves can be triggered by mechanical tidal oscillation or due to significant variation of latent heat. The convective system is, however, found as a major cause of such atmospheric acoustic wave (Baker and Davies, 1969; Hocke and Tsuda, 2001; Raju et al., 1981; Azeem et al., 2018; Walterscheid et al., 2003). The acoustic waves triggered by convective system oscillations at $\sim 10km$ altitude contains a significantly low amplitude variation. But, it propagates in the upward direction with a very high velocity and finally interacts with the charged atmospheric layers at lower/upper thermosphere with significantly high amplitude (Georges, 1968; Baker and Davies, 1969; Raju et al., 1981; Marshall and Snively, 2014).

Atmospheric gravity waves (AGW) can also originate due to various mechanisms such as atmospheric tidal oscillation, wind shear force (Hines, 1960), overshooting of convective thunderstorm system (Vadas and Fritts, 2004; Vadas et al., 2009) etc. The amplitude of such waves are usually large with a small wavelength. It breaks and dissipates at stratospheric and mesospheric altitude, but a small

* Corresponding author.
E-mail address: soumendatta88@gmail.com (S. Datta).

https://doi.org/10.1016/j.asr.2023.09.018
0273-1177/

portion of these waves manages to reach the thermospheric altitude via various atmospheric filtering process such as chemical loss, photo ionization, or other dynamic processes. Such waves generally achieve significantly high phase velocity and large vertical wavelength after reaching the thermospheric altitude. Both, Kinematic viscosity and thermal diffusivity play important roles in AGW propagation as dissipative filter at thermospheric altitude because of the rapid decay of the atmospheric neutral density and increase of temperature respectively. The uni-directional wind filtering along with the dissipative filtering eliminate a significant spectrum of such low frequency waves that reach this altitude. The rest can be traced by the perturbation in ion density due to the interaction with the ionosphere which has been evidenced by several in situ measurements. Substantial evidences have been reported by several researchers on perturbation of these waves in lower ionospheric layers (Lay and Shao, 2011; Yue et al., 2013; Rahmani et al., 2020) and F layer (Fritts et al., 2008; Vadas and Liu, 2013; Jaroslav et al., 2021). Maurya et al. (2022) found a rare event of simultaneous occurrance of sprites and gravity waves at ionophseric D, E and F region. Chowdhury et al. (2023)have done a statistical study on the thunderstorm activity and induced gravity wave signature at the ionospheric region. They found a novel correlation between the peak lightning stroke intensities and the travelling ionospheric disturbances amplitude. Sometimes, wave variations with comparatively larger frequency (4 to 15 mHz) associated with various convective system, have also been observed at the ionospheric altitude (Baker and Davies, 1969; Marshall and Snively, 2014; Lay, 2018; Azeem et al., 2018) and it is considered as the consequence of acoustic wave. However, the characterization of the acoustic wave is difficult due to the lack of numerical assessment and theoretical study, but these waves have been found to transfer a significant amount of heat energy to the thermosphere by the viscous dissipation and wave energy. Hence the acoustic wave has a significant contribution to heat the thermosphere whereas the gravity wave has the cooling effect (Hickey et al., 2001).

The study of low frequency neutral wave propagation can be attempted by studying two different phenomenon in the atmosphere i.e., the rapid fluctuation of neutral gas molecules and the plasma perturbation in the charged atmosphere (Hocke and Schlegel, 1996). The measurements on the first mechanism happens to be very much demanding in nature due to requirements of various complex instrumental set up (Natorf and Schlegel, 1992). The second method can therefore facilitate as a very useful and popular technique for such neutral wave dynamics.

The availibility of satellite navigation systems by several nations and installation of closely spaced receivers make the investigation on neutral as well as the charged atmospheric layers highly benefecial. Presently, the two-dimensional ionospheric total electron content (TEC) product based on the measurements from these receiver network can be utilized for various space weather related studies as well as the understanding of the coupling process between various layers of the atmosphere. Observation of wave like pattern in ionospheric TEC measurement after various natural hazards is very common. The tracing of ionospheric acoustic waves using navigation signal have been carried out by several authors (Saito et al., 2011; Lay et al., 2015; Lay, 2018; Rahmani et al., 2020). Various statistical studies have also been done based on these acoustic waves which were triggered by convective system and other natural hazards and traced at ionospheric altitudes (Xiao et al., 2007; Lay et al., 2015; Berngardt et al., 2017). These statistical observations along with the theoretical studies indicate that these acoustic waves cannot propagate large distance from the thunderstorm affected area and attenuate heavily after reaching the thermospheric altitude due to thermal conductivity and molecular viscosity (Walterscheid et al., 2003; Chum et al., 2012; Berngardt et al., 2017). Walterscheid et al. (2003), Lay et al. (2015) also mentioned that thermospheric temperature gradient plays a key role to prevent the acoustic waves in reaching the ionospheric altitude. In comparison to that, gravity waves travel through dissipative filtering in thermospheric altitude where they dissipate at lower thermosphere and generate secondary gravity waves (Vadas, 2007; Vadas and Azeem, 2021). Hence it is noteworthy to find the acoustic wave signature associated with the convective system in the tropical region because of the very high thermospheric temperature gradient in this region.

The current study has focused on wave like perturbation signature in ionospheric total electron content measurement by using NavIC signal during severe thunderstorm systems observed on consecutive two days March 31 and April 1, 2018. The application of NavIC signal has been proven for ionospheric studies and for other fields as well (Chakraborty et al., 2020; Desai and Shah, 2018; Kumar et al., 2019; Ayyagari et al., 2020; Das et al., 2020; Ayyagari et al., 2023). Different types of TID signatures containing high frequency components (~ 5 mHz) have been observed in some cases as the consequence of acoustic wave interaction with ionosphere whereas; very strong lower frequency (lower than 2 mHz) responses due to the gravity wave were witnessed in many occasions. This is a very rare opportunity to find both such wavefront signatures caused by the thunderstorm system in the tropical region. Only a very few events of acoustic waves triggered by thunderstorm system in tropical region are found so far (Raju et al., 1981; Walterscheid et al., 2003; Lay, 2018). It is noteworthy to mention both these wavefronts have been detected by using newly launched NavIC signal which is strengthened by similar signatures obtained in the GPS signal, tracked by nearby GPS receivers. The study has been done based on the measurements by a single NavIC receiver. Hence the details wave characteristics for which at least three receivers are required, could not be retrieved from the NavIC signal in the present study. But the NavIC signatures along with substantial evidences indicate the

potential of NavIC signal to investigate the wave characteristic more precisely.

2. Data and methodology

The lightning information is used as a proxy of thunderstorm intensity but the dynamicity of the process doesn't allow to study the generation and propagation of the acoustic/gravity wave. Lightning measurements are taken from ground lightning network WWLLN database [http://wwlln.net/]. WWLLN is a global lightning network which is operating at VLF frequency bandwith and collecting data from 70 stations around the globe. The network detects the location of every lightning strike and provides its energy. It measures the sferics in the VLF band due to a lightning flash from 3 or more stations.

Dual frequency navigation data has been collected from two different types of receivers. GPS data has been obtained from UNAVCO archive [https://www.unavco.org/]. NavIC data for this study has been collected by an NavIC/GPS/SBAS SPS receiver (model: ACCORD) which can acquire NavIC (dual frequency L5 and S1), GPS (single frequency L1) and SBAS (GAGAN) signal. NavIC is the regional navigation satellite system over the Indian subcontinent with its seven-satellite constellation of which four are geosynchronous and three are geostationary. It facilitates real time standard positioning service operated at two different frequency band L5 (1176.45 MHz) and S1 (2492.028 MHz). The location of all receiver are listed in Table 1.

Ionospheric perturbation has been computed based on the trend of the total electron content instead of its absolute measurement. The biasing components can be solely neglected for our methodology because its slowly changing components does not affect the relative TEC measurements in short duration. The trend of the local ionospheric TEC is calculated based on the difference of the carrier phase delays measured in two different frequencies:

$$s = \left[\frac{L_1 - L_2}{k}\right] + b \tag{1}$$

where L1 and L2 are the carrier phase delay measurements in two different frequencies, k is the conversion factor to convert the phase delay to VTEC measurement, b is the biasing error mixed in carrier phase delay. The utilization of carrier phase delay is highly beneficial as it is very less noisy compared to the pseudorange. But the carrier phase delay for NavIC signal specially measurement in S1 band significantly suffer from cycle slips which causes unconditional jumps between two epochs. These cycle slips are needed to be detected and corrected accurately for the perturbation estimation. Here, Melbourne-Wubbenna (MW) Combination based on wide lane carrier phase delay and narrow lane pseudorange combination has been used for its reported efficiency in detection of cycle slips (Dach et al., 2015; Bezmenov et al., 2019). Two algorithms have been applied here for cycle slip detection. 1) The time series of MW combination is estimated based on the carrier phase delay and pseudorange measurements. The study has been carried out considering epochs of certain length L (here 480 sample length is considered). Initially, the standard deviation of MW combination within this time length has been computed. Next, for each i-th value in this length, it has been verified if the running deviation (deviation of i-th value from mean of 1 to (i-1)-th value) crossed the standard deviation. This hints towards the presence of a cycle slip. 2) An elevation dependent weighting function ($exp^{-elv/10}$) is used here for further confirmation of cycle slip. A cycle slip is anticipated if the difference between two consecutive values in carrier phase exceeds the mentioned weighting function. If both the above algorithms satisfy at a particular interval, then a slip of cycle is confirmed. The entire data processing is done based on the methodologies given in Dach et al. (2015), Blewitt (1990), Springer (2000). After successful removal of the cycle slip, differential TEC (dTEC) is estimated based on the carrier phase difference as mentioned in Lay et al. (2013), Lay (2018), Ayyagari et al. (2023).

Table 1
Location of NavIC and GPS receivers.

Receiver Name	System	Latitude	Longitude
ACCORD Kolkata	NavIC	22.65°N	88.4°E
PD32	GPS	22.50°N	89.43°E
HRNP	GPS	21.81°N	89.46°E
DHAK	GPS	23.73°N	90.40°E
CHNR	GPS	24.19°N	91.51°E
SSPS	GPS	24.28°N	91.89°E

3. Results

The Intertropical Convective Zone (ITCZ) line passes through the central part of India. The landmass over the eastern parts of the country faces a large temperature difference w.r.t sea which makes it prone to cyclonic movements. This region witnesses extremely high lightning activities especially during the pre-monsoon season due to cyclonic movements in Bay of Bengal. Besides, the study location Kolkata (22.6488°N and 88.3770°E) is located at lower Ganges delta of eastern India and is chosen due to its frequent weather extremity. Frequent lightning event occurs during the pre-monsoon (May-June) and post-monsoon (September) time. Here, Nor'westers, the frequent extreme weathers, cause huge damage to property and human lives by lightning events and strong squalls.

Two such thunderstorm systems developed over the study location in consecutive two days, March 31 and April 1, 2018. The Dst index shows that that the minimum level it went down to −5nT as shown in Fig. 1. It indicates that no such geomagnetic disturbances occurred during these two days. The variations of Kp and ap indices are also indicative for calm geomagnetic condition. A large number of

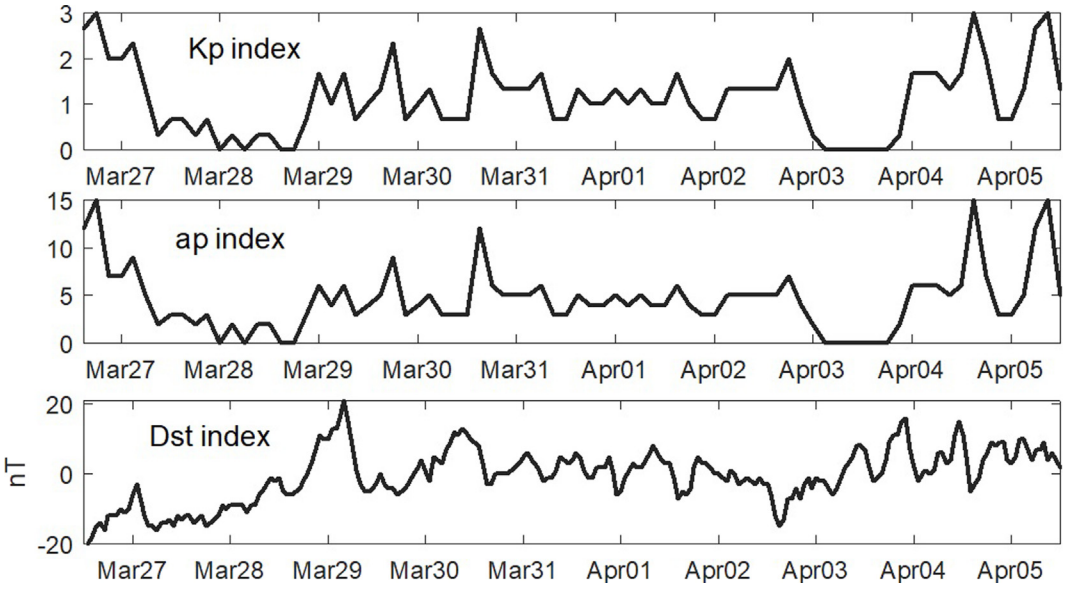

Fig. 1. Kp, ap and, Dst indices for 31st March and 1st April.

lightning strikes occurred due to these thunderstorm systems in both days. Fig. 2(a) shows the lightning strike locations on March 31, 2018 which indicates that a significant number of strikes occurred over a small area of the Eastern part of India. The temporal distribution of strikes as shown in Fig. 2(b) indicates that most of the strikes occurred during UTC 1 to 4Hr. and UTC 09 to 15Hrs. A major convective system developed on April 1, 2018 also covering a vast region along the eastern coast of India. A significant number of lightning strikes occurred over the affected area. Fig. 2(c) and (d) shows the lightning affected area and the strike count variation with time. It indicates that the

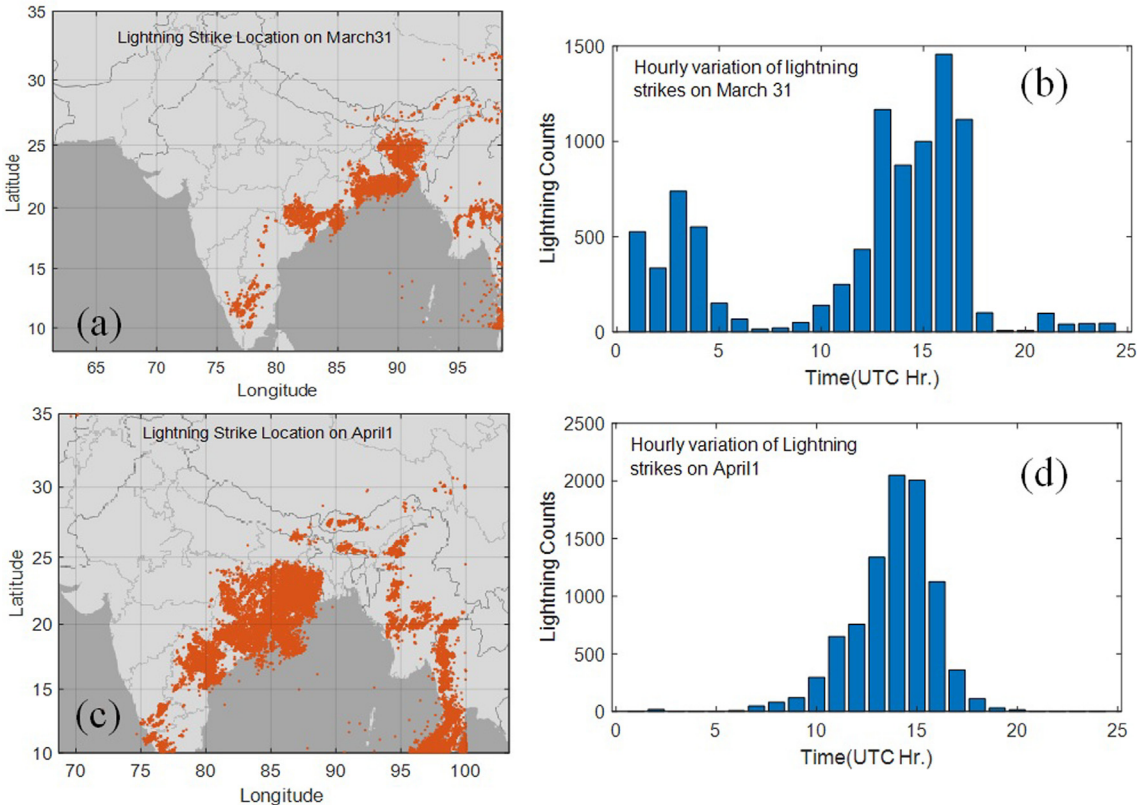

Fig. 2. WWLLN lightning strike information over the study location (a) Lightning strokes location and (b) Hourly variation of lightning strikes on March 31, 2018. (c) and (d) are same as (a) and (b) respectively for April 1, 2018.

event started at 07:00 UT and continued till 21:00 UT and reached its peak at around 14:00–15:00 UT.

Differential TEC, as measured by each of the six NavIC satellite signal have been presented in Fig. 3 for continuous 5 days from March 31 to April 4. Being a GEO-constellation (combination of both geostationary and geosynchronous), it offers a rare opportunity to track a particular event on the earth through a single satellite throughout a sidereal day. Significant TID signatures were identified on both 31March and 1st April in all NavIC satellites and they gradually decreased for the next consecutive days. On April 2 some small signatures were there which can be attributed as the effect of thunderstorm induced gravity wave for a longer time. No such signatures were identified in the next two days and the maximum amplitude was within ±0.15 TECU.

3.1. Ionospheric perturbation signature on March 31, 2018

A notably strong signature of perturbation had been obtained from 10:00 UT in each signal and the amplitude of fluctuation were found to be within ~0.5 to 0.8 TECU (Fig. 4). All the satellites except IRNSS 1C and 1E showed significantly low amplitude dTEC variation (~ 0.1 TECU) before 04:00 UT. Therefore, the noise threshold in dTEC measurements can be considered as 0.1TECU. The noise characteristics in dTEC measurements from NavIC satellites are mostly similar to GPS and the threshold of the noise has been considered as ±0.1 TECU after a long term observation. Interestingly, the TEC fluctuation settled down to the threshold level after 16:00 UT. It is therefore evident that the irregularity in TEC were observed in the post-development phase of the thunderstorm system. However, the initiation of the irregularity occurred at different times for different satellites according to their respective positions and movement of the system.

3.1.1. Signature of acoustic wave

The above findings interested us towards a deeper insight into the frequency response of TIDs observed. The frequency spectrum for all the TIDs showed a common (and dominating) frequency component of 0.1 cycle/min. IRNSS 1B, on the other hand, presented the evidence of a higher frequency component of around 0.3 cycle/min with significant high amplitude above the noise threshold level (green lines). This was evidenced in IRNSS 1C as well but with a smaller intensity (Fig. 5a). None of the other satellites had such high frequency components and the amplitude variations were also under the noise threshold. This falls in line with the location of IRNSS 1B and 1C whivh were close enough to the thunderstorm system developed (Fig. 6). A band pass filter has been applied next to separate out the acoustic waves. The filtered-out response in IRNSS 1B and 1C were found to be 0.3 and 0.2 TEC respectively at the higher frequency component whereas; rest of the satellite presented no such signature.

The study was repeated for GPS satellites which also showed similar results (Fig. 5b). IPPs near the mesoscale

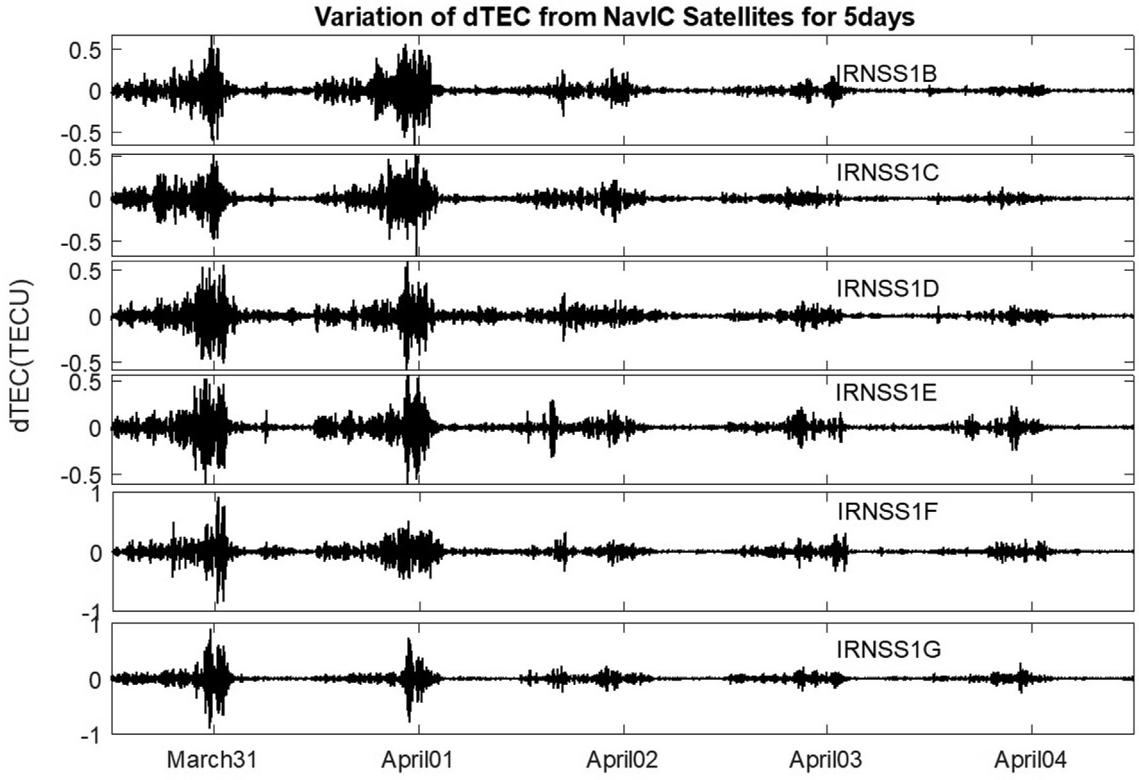

Fig. 3. The TID signature of six NavIC satellites for continuous 5 days (March 31 to April 04, 2018).

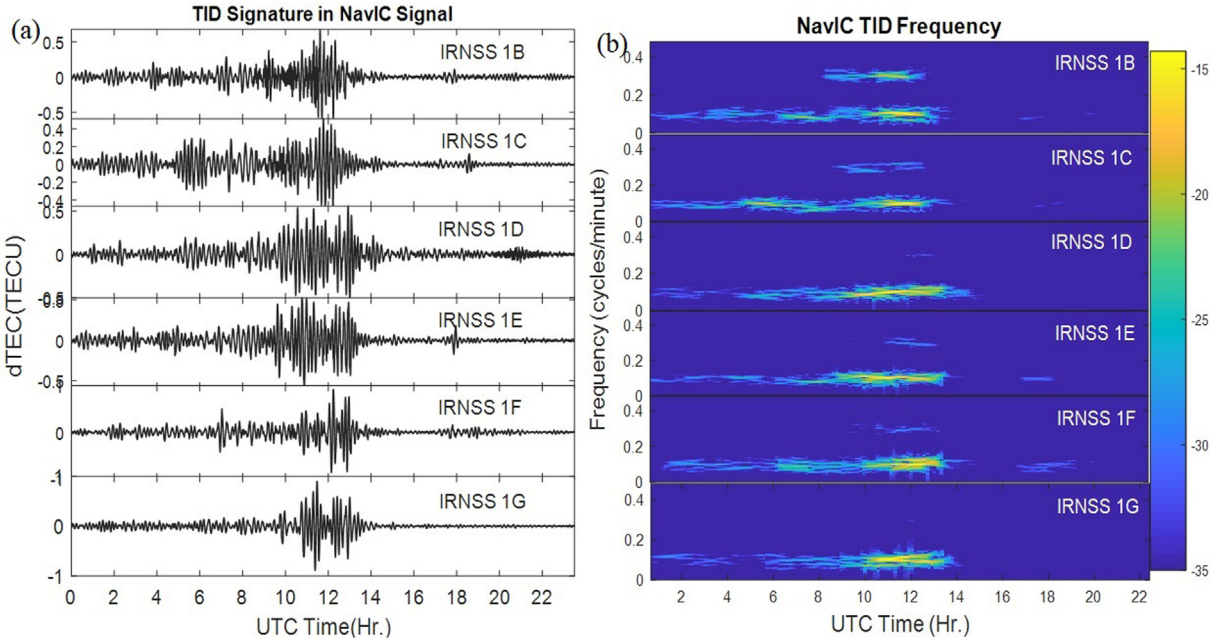

Fig. 4. TID signature from all six NavIC satellites measurements (a) amplitude variation of the TID measurements (b) frequency response of observed TID measurement.

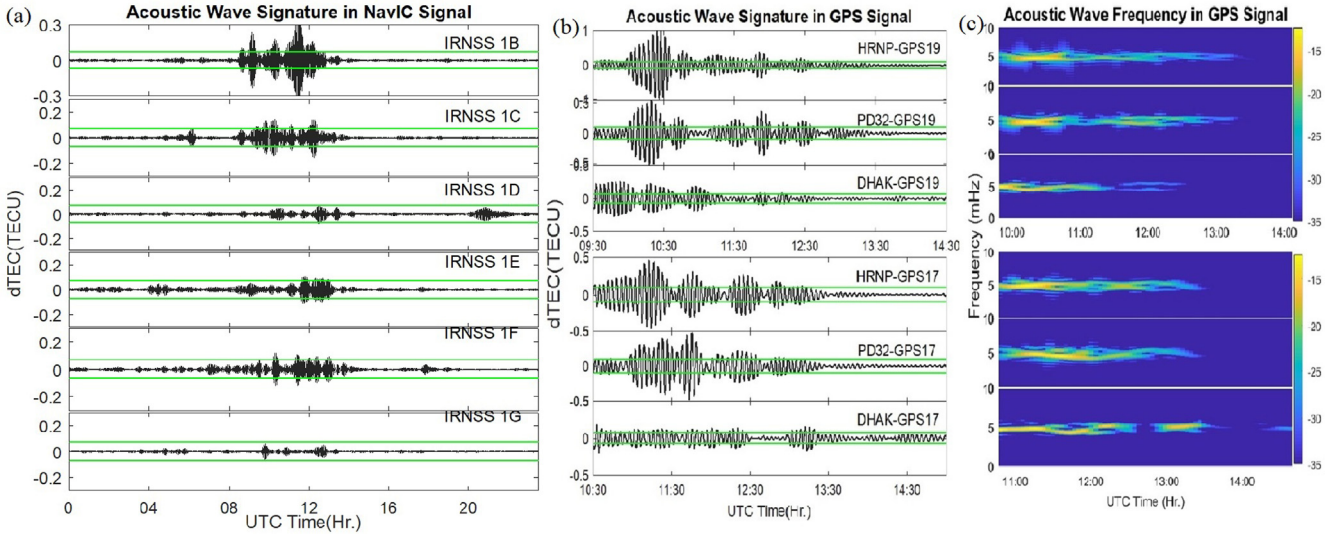

Fig. 5. Signature of Acoustic wave (green line indicates the threshold of noise for acoustic wave which is considered here 0.05TECU) (a) measurements from NavIC signal; (b) Measurements from GPS signal; (c) frequency response of acoustic wave retrieved from GPS signal.

system (HRNP GPS 19, PD32 GPS 19, HRNP GPS 17 and PD32 GPS 17) presented the evidence of the acoustic waves with significant intensity. A high frequency component of ~0.3 cycle/min (5 mHz) were observed in this case as well. The results were similar from two navigation systems of completely different constellations and operating frequencies strengthens the notion of thunderstorm driven acoustic waves in atmosphere of lower latitude region.

3.1.2. Gravity wave signature

The dominating frequency component as observed in each of the NavIC PRN is 0.1 cycle/min (~ 1.7 mHz) which speaks about the possibilities of a gravity wave being generated by the event (Fig. 7a) as well. Therefore, the signal has been passed through another band pass filter of 1 mHz-4 mHz bandwidth. A significant signature above the noise threshold with perturbation of around ±0.5 TECU was obtained in each of the satellite signal when passed through the filter. Similar patterns were observed in several GPS satellites (Fig. 7b and 7c). The fluctuations varied between 0.5 TECU - 0.8 TECU.

Unlike the short-lived acoustic waves, a gravity wave can propagate through a much longer distance and can persist in atmosphere for a longer span. Therefore, the sig-

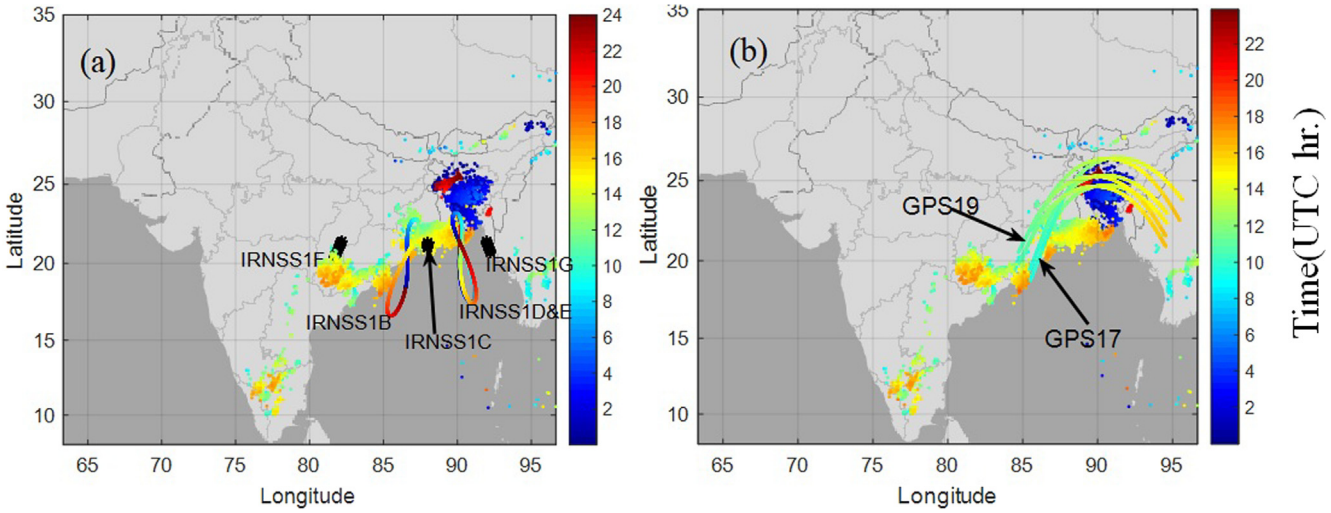

Fig. 6. IPP Location of NavIC and GPS satellites and lightning strike location; colours denote the UTC time (a) NavIC satellites; (b) GPS satellites.

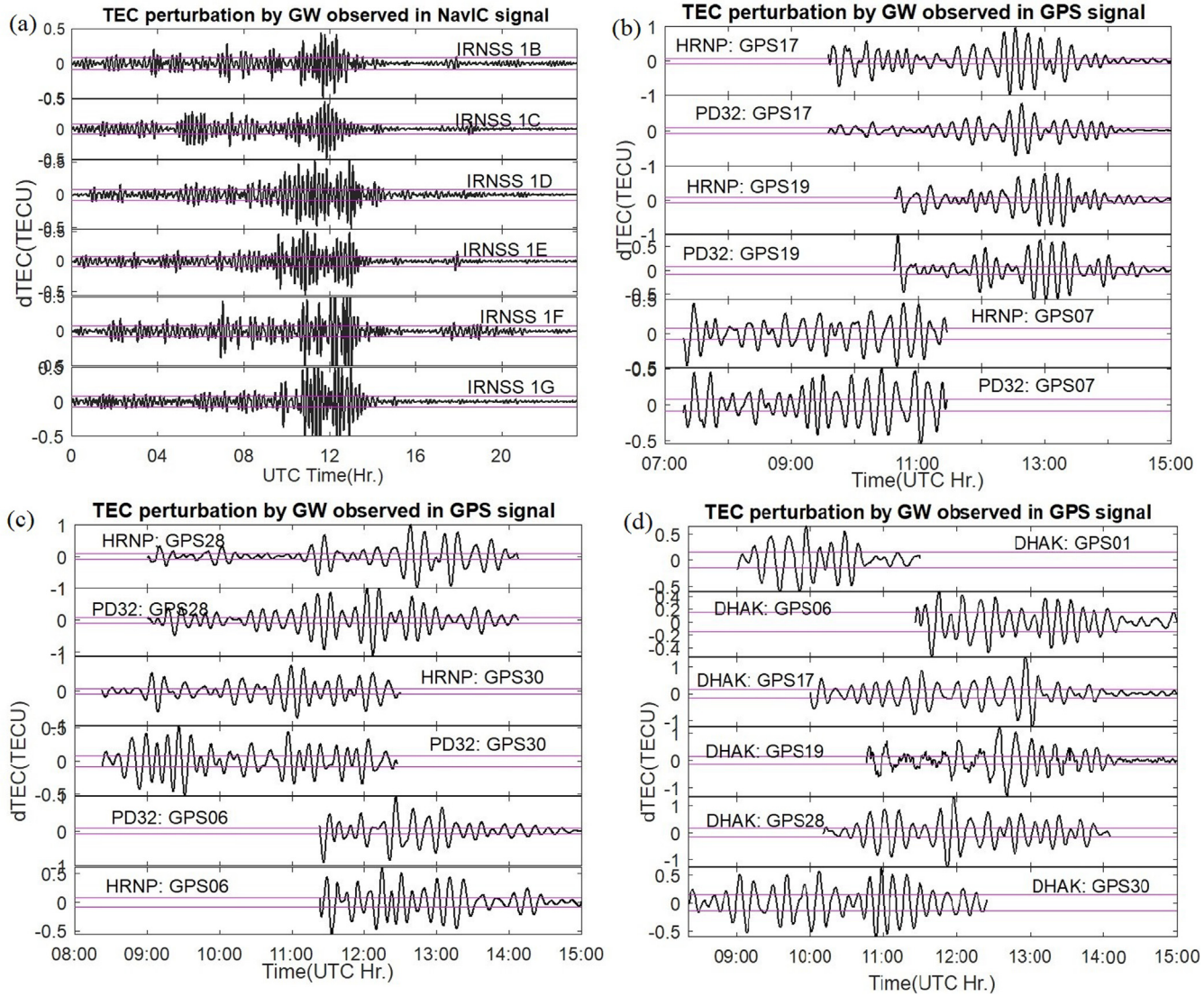

Fig. 7. Signatures of gravity wave (magenta line indicates the noise threshold for gravity wave measurements which is considered here 0.08TECU (Lay et al., 2015)) (a) Measurements from NavIC signal (b) and (c) Measurements from GPS signal.

nature of perturbations were captured equally well both by GPS and IRNSS signal in this case. The major sudden fluctuation in dTEC started after 10:00 UT in most of the satellites. Interestingly, the effect initiated much before in IRNSS 1C, 1D and 1F. It is to be noted, that even though the main phase of the event started after 09:00 UT there were significant amount of lightning activities during 01:00–05:00 UT as well. As a matter of fact, IRNSS 1C, 1D and 1F are in southern and south-west direction respectively and near to the mesoscale system (Fig. 6a) and during 01:00–05:00 UT the meridional wind was majorly northwards whereas; zonal wind was weak but eastward (Fig. 8a). The relation of vertical wavenumber and the horizontal wave number can be expressed as:

$$K_{\text{ver}}^2 = \frac{K_{\text{hrz}}^2 * N_B^2}{(\omega - K_{\text{hrz}} * U)^2} - K_{\text{hrz}}^2 - \frac{1}{4H^2} \quad (2)$$

K_{ver} and K_{hrz} are the vertical and horizontal wave numbers respectively, ω is the intrinsic frequency, U is the horizontal wind speed. Hence, the waves propagating along the direction of wind will dissipate due to the viscosity and their smaller vertical wavelength ($\lambda_{ver} = 2\pi/K_{ver}$). Hence, the meridional wind flowing in the opposite direction results in a increased vertical wavelength of the propagating gravity wave which eventually makes it more efficient in reaching ionospheric height (Vadas and Azeem, 2021).

3.2. Ionospheric perturbation signature on April 1, 2018

3.2.1. TID

Fig. 9 presents the variation in dTEC for each of the satellite. It is evident that all the satellite signal showed sudden fluctuation of dTEC starting at around 10:00 UT. The signature was, however, the strongest in IRNSS 1B and 1F. Moreover, the effect initiated much earlier (08:00 UT) in these two PRNs. The fluctuation in IRNSS 1C was weaker than these two but significantly stronger than the rest. The frequency response showed the dominance of 0.1 cycle/min component in most of the satellites. A higher frequency component (0.3 cycle/min) were observed in IRNSS 1B and 1F which was weaker in 1C but rest of the satellites are showing no such higher frequency responses.

3.2.2. Acoustic wave

The dTEC variation were passed through a bandpass filter to further investigate the presence of acoustic waves. The filter output strengthens the previous findings with strong signature of perturbation above the noise threshold in IRNSS 1B and 1F (Fig. 10a). The location of strikes and the IPP location of the satellites with time indicate that the location of the said NavIC satellites were very closely aligned to the lightning affected area whereas IRNSS1C is situated on the boundary of the affected area (Fig. 11. Similar investigation with GPS system reveals pretty comparable signature in PRN 19 and 17 in IPP location observed from HRNP, PD32 and CHNR because of their adjacence to the central part of the mesoscale system. It is to be noted, this thunderstorm system was much more intense than that reported on March 31. As a result, the evidence of acoustic waves in this case was much stronger.

3.2.3. Gravity wave

The majorly dominating frequency component in the spectrum of dTEC obtained from each of the IRNSS satellite was 1.7 mHz. The frequency of gravity wave happens to be below 4 mHz. Therefore, a bandpass filter of 1–4 mHz bandwidth was applied in the signal and the output is shown in Fig. 12. The output confirms strong signature of dTEC fluctuation (+/− 0.3–0.5 TECU) in each of the PRNs where IRNSS 1B and 1F showed the strongest ones. The pattern in these two satellites initiated earlier than the rest. The zonal wind speed was very high and westward in this case. The satellites were majorly located in the eastern direction which favours easy reach out to the ionospheric height due to the strong westward zonal wind at 10:00 UT as shown in Fig. 6. The wind pattern was also almost

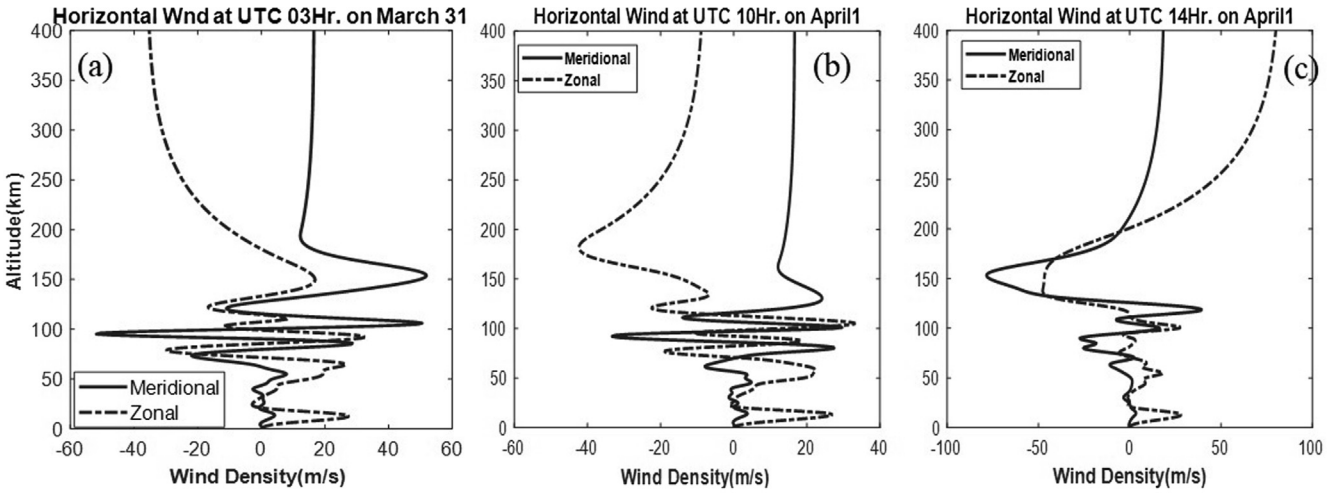

Fig. 8. Horizontal wind velosity from HWM14 model over the study location.

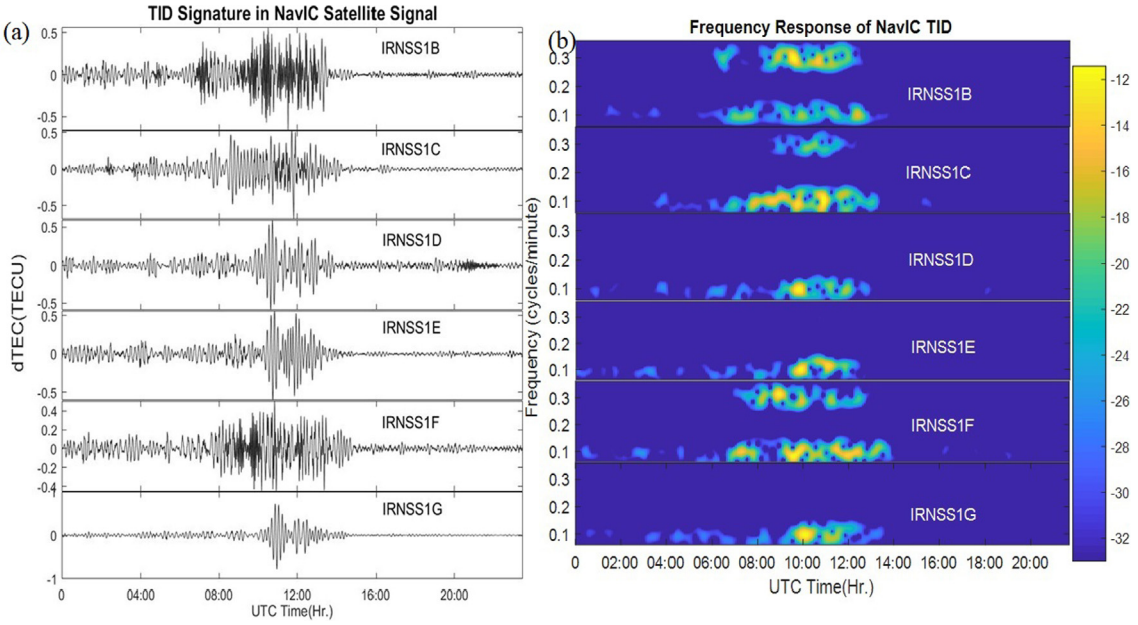

Fig. 9. TID signature from all six NavIC satellites measurements on April1 (a) amplitude variation of the TID measurements (b) frequency response of observed TID measurement.

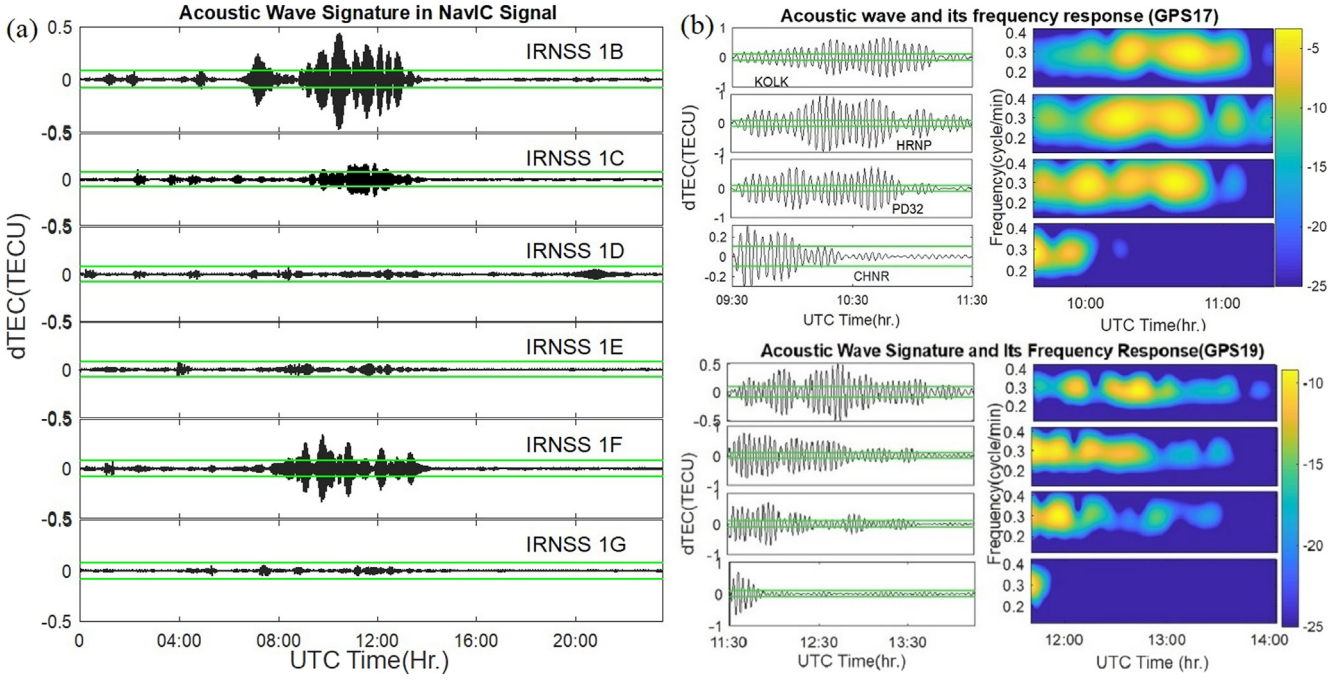

Fig. 10. Acoustic wave signature on April1(a) measurements from NavIC signal; (b) Measurements from GPS signal; (c) frequency response of acoustic wave retrieved from GPS signal.

similar 1hr. before and after (not shown in figure) that time. However, IRNSS 1B and 1F, being within the closest proximity of the thunderstorm system, presented the signature for longer duration.

The GPS satellites signal also showed significant effects. Measurements taken from PRN 06, 07, 17, 19, 28, 30 of HRNP, PD32 and CHNR receivers showed a notable perturbation effect which started from almost 09:00 UT and a strong effect was obtained after 11:00 UT. This is very similar to the signatures obtained from the measurements by NavIC signal. Interestingly the IPP location of the said satellites are towards the east direction. Hence, it indicates the potential of NavIC signal in thermospheric study and understanding of coupling process between atmospheric layers.

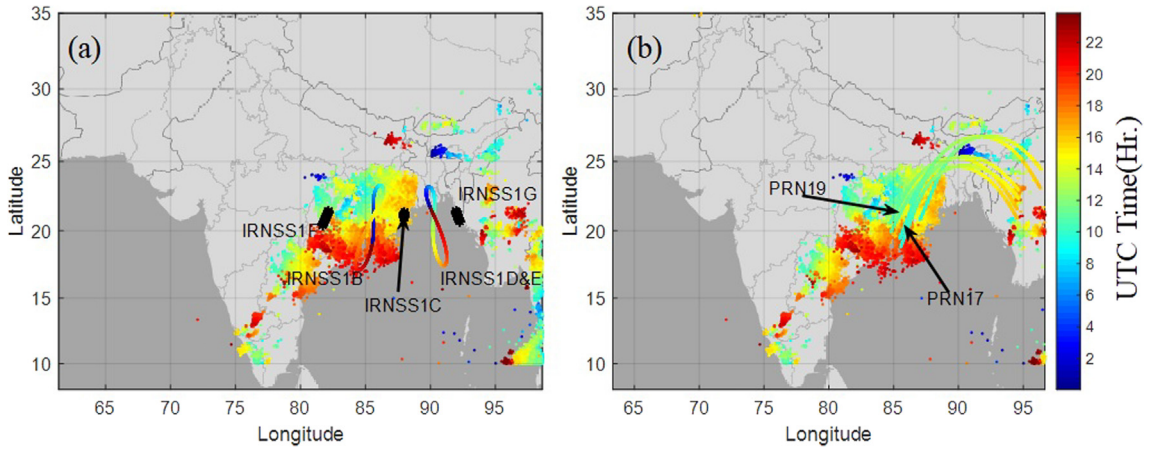

Fig. 11. IPP Location of NavIC and GPS satellites and lightning strike location on April1; colours denote the UTC time (a) NavIC satellites; (b) GPS satellites.

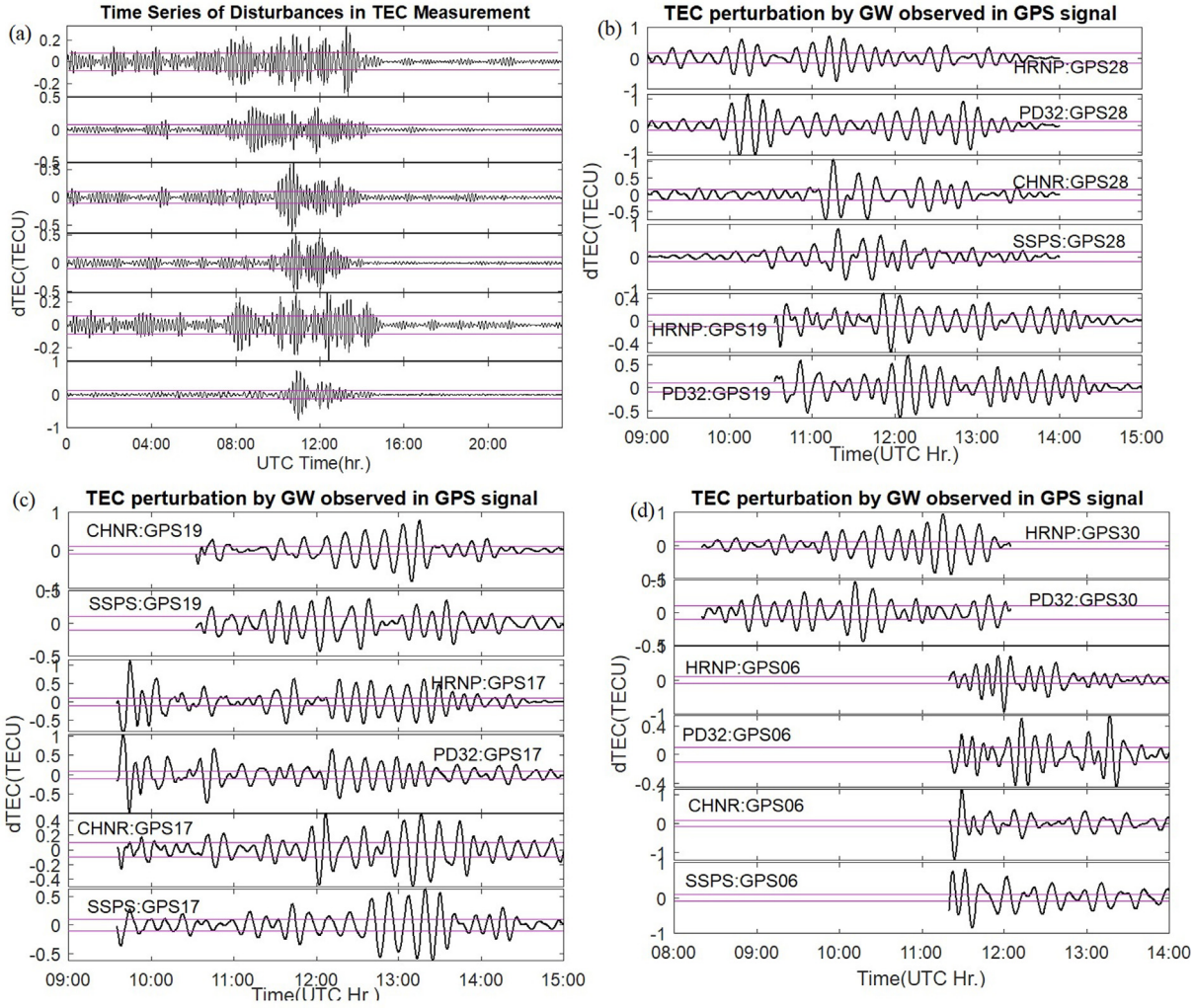

Fig. 12. Gravity wave signatures on April1(a) Measurements from NavIC signal (b) , (c) and (d) Measurements from GPS signal.

3.3. TID spectral power and lightning stroke energy density

Another investigation has been done separately on NavIC and GPS signal to find the relationship between the TID spectral power and lightning energy density. The TIDs of the respective satellites are chosen that passes within 300 km radius of the maximum stroke density region as mentioned in Chowdhury et al. (2023). The spectral density of the TID is measured based on continuous wavelet transform and average strike energy is calculated based on the total strike energy divided by number of strikes inside $1^\circ \times 1^\circ$ spatial bin. Fig. 13 shows that the relation between these two parameters seems linear, but the correlation coefficients (64%) are not significant to draw any conclusion. It may be due to the small number of samples or the background neutral as well as charged atmospheric conditions. Hence, a more detail study is required which is out of scope for this present study.

4. Discussion and conclusion

This article reports two rare events of thunderstorm generated acoustic wave in travelling ionospheric disturbances at Indian region. Studies reporting ionospheric acoustic waves generated by convective events at the tropical region are extremely rare (Lay, 2018), even though such studies are abundant in mid-latitude region (Davies and Jones, 1973; Lay et al., 2015; Saito et al., 2011; Zettergren and Snively, 2013). This is due to the changes in plasma characteristics as well as neutral atmospheric condition. In low-latitude region, the plasma behaviours are driven by complicated electrodynamics in presence of large scale electric fields. Hence, a higher plasma motion and turbulent nature is observed in low-latitude ionospheric F Layer (Fejer, 1981; Forbes, 1981). Equatorial plasma bubble and ionospheric scintillation are the two most common outcomes, which are observed in equotorial ionosphere. Tang et al. (2019), Kumar et al. (2017) reported strong scintillation and plasma bubble at low-latitude ionosphere after severe thunderstorm. The neutral background component such as themospheric temperature gradient also plays a key role to prevent the acoustic wave to reach the ionospheric altitude (Lay et al., 2015). Hence, in this context wave like nature in sporadic tropical ionospheric layers is extremely rare and challenging to detect. Here, clear signatures of ~ 5 mHz frequency component with 0.4 TECU amplitude variation have been detected in both NavIC and GPS TID measurements as the consequence of acoustic wave interaction with ionosphere after severe lightning strikes in the reported two cases. Walterscheid et al. (2003), Lay et al. (2015), Lay (2018) also reported the presence of similar high frequency TIDs during severe convective systems. The acoustic waves are detected only inside a very short radial range from heavily lightning affected area. Interestingly, the enhancement of acoustic wave signature with the increase of the thunderstorm activity was also witnessed.

On the other hand, gravity wave signatures are not that uncommon. The gravity waves are primarily triggered by overshooting of convective plume into the stratosphere and propagate in upward direction with increasing amplitude. A significant number of these GWs with higher amplitude and small vertical wavelength breaks before mesopause. But the investigations have also revealed the broad spectrum of the gravity wave activity from the lower atmospheric convective sources to the thermosphere and ionosphere as well. Though there is also high possibility of secondary gravity wave generation at the thermospheric altitude, but the amplitudes of these secondary gravity waves are very less compared to the waves propagating at the mesospheric altitude. After dissipating through the process of momentum deposition, another waveform is excited at thermospheric altitude which has small amplitude and higher vertical wavelength. This part of wave is called secondary wave and has wide spectral range and propagates with high phase velocity at the thermospheric altitude. It also leaves its signature on the plasma distribution of the charged medium by producing the travelling ionospheric disturbances through ion-neutral collision process. Besides, the study location is situated at the sub-

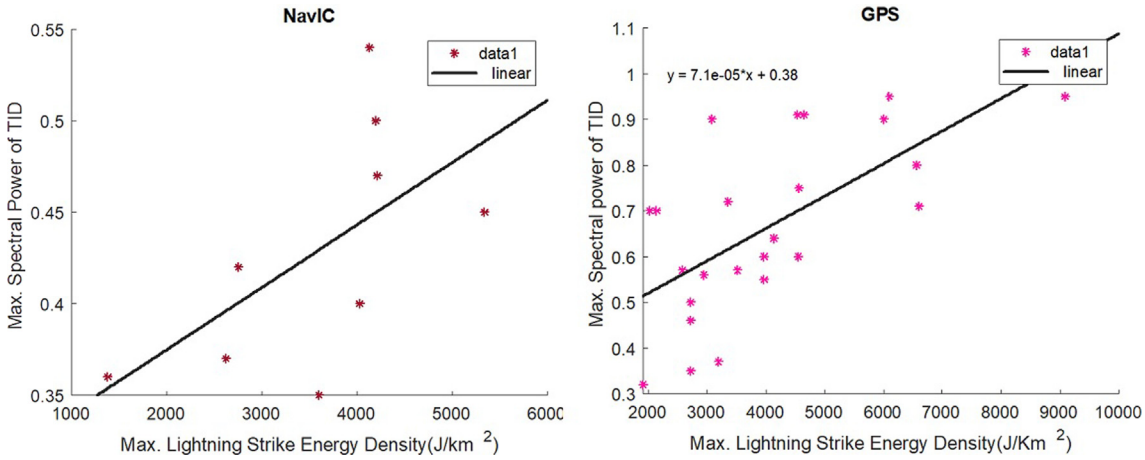

Fig. 13. Relationship between max. lightning strike energy density and TID spectral power of NavIC and GPS signal.

tropical region where several types of irregularities such as scintillation, bubbles are always present in the ionospheric plasma distribution, which make it very difficult to detect the secondary waves induced perturbation. There can be a few other factors which can also play a role behind the uncertainties in detection of secondary gravity wave response over the ionospheric plasma distribution which includes deficiency in number of reference receives for continuous monitoring in all directions, the time of occurrence of convective sources (amplitude of perturbation become significantly smaller after post evening period as compared to midnoon time), longitudinal variability from the sources etc.

Several past studies reported the gravity wave signatures at the low-latitude region (Kumar et al., 2017; Lay, 2018; Tang et al., 2019; Ogunsua et al., 2020; Liu et al., 2021). The background horizontal wind neutral atmospheric density and thermospheric temperatures play key role for the propagation of gravity wave. The horizontal wind flow opposite to the direction of gravity wave propagation increases the vertical wavelength which favours its propagation towards higher altitude. The exponential decay of atmospheric neutral density with altitude at thermosphere increases the kinematic viscosity largely. Thermal conductivity also becomes significant due to the rapid increase of temperature at thermosphere. The two said parameters act as tuning factors in dissipative filtering process (Vadas and Fritts, 2005). Hence the gravity wave propagating upward direction dissipates at lower thermosphere and generates a secondary gravity wave (Vadas et al., 2019; Vadas and Azeem, 2021). Significant gravity wave signatures have been detected in both NavIC and GPS TID measurements. The signatures are found to correlate very well with the thunderstorm activities. Horizontal wind has also seemed to play a key role in TID signatures. The horizontal wind measurements in the opposite direction of gravity wave flow from the lightning affected area shows a significant TID amplitude. A large attenuation effect is also observed along the wind direction. However, the current study could not compute the circular or semi circular rings of TID signatures which are generally produced by concentric source of gravity wave due to the lack of availability of sufficient number of GPS and NavIC receiver data. The limitation also impacts the continuous observations between 0 to 360°azimuthal angle. It might cause some temporal miss-alignments between the peak lightning activities and gravity wave responses at ionospheric altitude during both the observation days. The previous investigations also reported that maximum perturbations in ionospheric TEC measurements caused by lower atmospheric convective sources, happen from local noon to pre-evening time and after that the perturbation amplitude decreases (Vadas et al., 2014; Nigussie et al., 2022). As the peak lightning activities occurred much later than the post-evening time over the study location, this might cause the reduction of perturbation amplitude. Hence, it's not possible to get an exact match between the peak lightning activities and ionospheric perturbation. However, that doesn't hinder the theory of the perturbation due to thunderstorm. The investigation of temporal connection will be an excellent future goal.

The other focus of this study to understand the capabilities of NavIC in the study of gravity waves. Since the NavIC constellation is markedly different from that of GPS or any other navigation satellite systems, the performance analysis of NavIC in such study is essential. Here we have presented two case studies from GPS and NavIC. There is no significant characteristics difference observed between the primary observations from NavIC and GPS signal. However, a single GPS satellite can measure the GW for very short duration while the individual NavIC satellite can monitor the same for a longer duration. This is because the use of geostationary and geosynchronous orbits in NavIC. It also facilitates to monitor the TID launching time more accurately. Besides that, the IPP velocity of NavIC is very low due to the use of GEO satellites in the constellation. This can facilitate better monitoring of wave propagation in thermospheric regions.

Declaration of Competing Interest

The authors declare that they have no known competing financial interests or personal relationships that could have appeared to influence the work reported in this paper.

Acknowledgments

Authors thankfully acknowledge The Environmental Planning and Coordination Organization (EPCO) Bhopal, Madhya Pradesh, India for funding this study under the Chief Minister Scholarship for PhD program. Authors also thankfully acknowledge Space Application Center (SAC), ISRO to provide ACCORD Receiver under NavIC/GAGAN utilization program (NGP-1). Authors would also like to acknowledge WWLLN for providing the lightning data.

References

Ayyagari, D., Chakraborty, S., Das, S., et al., 2020. Performance of navic for studying the ionosphere at an eia region in india. Adv. Space Res. 65 (6), 1544–1558. https://doi.org/10.1016/j.asr.2019.12.019, URL: http://www.sciencedirect.com/science/article/pii/S0273117719309044.

Ayyagari, D., Datta, S., Das, S., et al., 2023. Ionospheric response during tropical cyclones - a brief review on amphan and nisarga. Adv. Space Res. 71 (6), 2799–2817. https://doi.org/10.1016/j.asr.2022.11.026.

Azeem, I., Walterscheid, R.L., Crowley, G., 2018. Investigation of acoustic waves in the ionosphere generated by a deep convection system using distributed networks of gps receivers and numerical modeling. Geophys. Res. Lett. 45 (16), 8014–8021. https://doi.org/10.1029/2018GL078107.

Baker, D.M., Davies, K., 1969. F2-region acoustic waves from severe weather. J. Atmos. Terr. Phys. 31 (11), 1345–1352.

Berngardt, O.I., Perevalova, N.P., Podlesnyi, A.V., et al., 2017. Vertical mid scale ionospheric disturbances caused by surface seismic waves

based on irkutsk chirp ionosonde data in 2011–2016. J. Geophys. Res. Space Phys. 122 (4), 4736–4754. https://doi.org/10.1002/2016JA023511.
Bezmenov, I.V., Blinov, I.Y., Naumov, A.V., et al., 2019. An algorithm for cycle-slip detection in a melbourne–wÜbbena combination formed of code and carrier phase gnss measurements. Meas. Tech. 62 (5), 415–421. https://doi.org/10.1007/s11018-019-01639-5.
Blewitt, G., 1990. An automatic editing algorithm for gps data. Geophys. Res. Let. 17 (3), 199–202. https://doi.org/10.1029/GL017i003p00199.
Chakraborty, S., Datta, A., Ray, S., 2020. Comparative studies of ionospheric models with gnss and navic over the indian longitudinal sector during geomagnetic activities. Adv. Space Res. 66 (4), 895–910. https://doi.org/10.1016/j.asr.2020.04.047.
Chowdhury, S., Kundu, S., Ghosh, S., et al., 2023. Statistical study of global lightning activity and thunderstorm-induced gravity waves in the ionosphere using wwlln and gnss-tec. J. Geophys. Res.: Space Phys. 128 (1). https://doi.org/10.1029/2022JA030516, e2022JA030516.
Chum, J., Hruška, F., Zedník, J., et al., 2012. Ionospheric disturbances (infrasound waves) over the czech republic excited by the2011 tohoku earthquake. J. Geophys. Res. 117 (08), A08319. https://doi.org/10.1029/2012JA017767.
Dach, R., Andritsch, F., Arnold, D. et al., 2015. Bernese gps software, ver. 5.2. Astronomical Institute, University of Bern.
Das, S., Datta, S., Shukla, A.K., 2020. Detection of thunderstorm using indian navigation satellite navic. IEEE Trans. Geosci. Remote Sens. 58 (5), 3677–3684. https://doi.org/10.1109/TGRS.2019.2960035.
Davies, K., Jones, J.E., 1973. Acoustic waves in the ionospheric f2-region produced by severe thunderstorm. J. Atm. Terr. Phys. 35 (10), 1737–1744. https://doi.org/10.1016/0021-9169(73)90052-4.
Desai, M., Shah, S.N., 2018. Impacts of intense geomagnetic storms on navic/ irnss system. Annals Geophys. 61 (5). https://doi.org/10.4401/ag-7856, 557–557.
Fejer, B.G., 1981. The equatorial ionospheric electricfield. A review. J. Atm. Terr. Phys. 43 (5–6), 377–386.
Forbes, J.M., 1981. The equatorial electrojet. Rev. Geophys. 19 (3), 469–504. https://doi.org/10.1029/RG019i003p00469.
Fritts, D.C., Vadas, S.L., Riggin, D.M., et al., 2008. Gravity wave and tidal influences on equatorial spread f based on observations during the spread f experiment (spreadfex). Ann. Geophys. 26 (11), 3235–3252. https://doi.org/10.5194/angeo-26-3235-2008.
Georges, T.M., 1968. Hf doppler studies of traveling ionospheric disturbances. J. Atmos. Terr. Phys. 30 (5), 735–746.
Hickey, M.P., Schubert, G., Walterscheid, R.L., 2001. Acoustic wave heating of the thermosphere. J. Geophys. Res. 106 (A10), 21543–21548. https://doi.org/10.1029/2001JA000036.
Hines, C.O., 1960. Internal atmospheric gravity waves at ionospheric heights. Can. J. Phys. 38, 1441–1481. https://doi.org/10.1139/p60-150.
Hocke, K., Schlegel, K., 1996. A review of atmospheric gravity waves and traveling ionospheric disturbances: 1982–1995. Annals. Geophysics. 14, 917–940. https://doi.org/10.1007/s00585-996-0917-6.
Hocke, K., Tsuda, T., 2001. Gravity waves and ionospheric irregularities over tropical convection zones observed by gps/met radio occultation. Geophys. Res. Lett. 28 (14), 2815–2818. https://doi.org/10.1029/2001GL013076.
Jaroslav, C., Podolska, K., Rusz, J., et al., 2021. Statistical investigation of gravity wave characteristics in the ionosphere. Earth, Planets Space 73 (60), 1–16. https://doi.org/10.1186/s40623-021-01379-3.
Kumar, R., Miriyala, S., Ratnam, V., et al., 2019. Estimation of ionospheric gradients and vertical total electron content using dual-frequency navic measurements. Astrophys. Space Sci. 364 (49), 1–9. https://doi.org/10.1007/s10509-019-3535-y.
Kumar, S., Chen, W., Chen, M., et al., 2017. Thunderstorm/lightning-induced ionospheric perturbation: An observation fromequatorial and low-latitude stations around hong kong. J. Geophys. Res.: Space Phys. 122 (8), 9032–9044. https://doi.org/10.1002/2017JA023914.
Lay, E.H., 2018. Ionospheric irregularities and acoustic/gravity wave activity above low-latitude thunderstorms. Geophys. Res. Lett. 45 (1), 90–97. https://doi.org/10.1002/2017GL076058.
Lay, E.H., Shao, X.M., 2011. High temporal and spatial resolution detection of d-layer fluctuations by using time-domain lightning waveforms. J. Geo phys. Res.: Space Phys. 116 (A01317), 1967–1976. https://doi.org/10.1029/2010JA016018.
Lay, E.H., Shao, X.-M., Carrano, C.S., 2013. Variation in total electron content above large thunderstorms. Geophys. Res. Lett. 40 (10), 1945–1949. https://doi.org/10.1002/grl.50499.
Lay, E.H., Shao, X.M., Kendrick, A.K., et al., 2015. Ionospheric acoustic and gravity waves associated with midlatitude thunderstorms. J. Geophys. Res.: Space Phys. 120 (7), 6010–6020. https://doi.org/10.1002/2015JA021334.
Liu, T., Yu, Z., Ding, Z., et al., 2021. Observation of ionospheric gravity waves introduced by thunderstorms in low latitudes china by gnss. Remote Sens. 13 (20), 4131. https://doi.org/10.3390/rs13204131.
Marshall, R.A., Snively, J.B., 2014. Very low frequency subionospheric remote sensing of thunderstorm-driven acoustic waves in the lower ionosphere. J. Geophys. Res. Atmos. 119 (9), 5037–5045. https://doi.org/10.1002/2014JD021594.
Maurya, A.K., Parihar, N., Dube, A., et al., 2022. Rare observations of sprites and gravity waves supporting d, e, f-regions ionospheric coupling. Sci. Rep. 12 (581). https://doi.org/10.1038/s41598-021-03808-5.
Natorf, L., Schlegel, K., 1992. Gravity wave parameters derived from traveling ionospheric disturbances observations in the auroral zone. Radio Sci. 27 (6), 829–840. https://doi.org/10.1029/92RS01649.
Nigussie, M., Moldwin, M., Yizengaw, E., 2022. Investigating the role of gravity waves on equatorial ionospheric irregularities using timed/saber and c/nofs satellite observations. Atmosphere 13 (9), 1414–1437. https://doi.org/10.3390/atmos13091414.
Ogunsua, B.O., Srivastava, A., Bian, J., et al., 2020. Significant day-time ionospheric perturbation by thunderstorms along the west african and congo sector of equatorial region. Sci. Rep. 10 (8466). https://doi.org/10.1038/s41598-020-65315-3.
Rahmani, Y., Mahdi Alizadeh, M., Schuh, H., et al., 2020. Probing vertical coupling effects of thunderstorms on lower ionosphere using gnss data. Adv. Space Res. 66 (8), 1967–1976. https://doi.org/10.1016/j.asr.2020.07.018.
Raju, D.G.K., Rao, M.S., Rao, B.M., et al., 1981. Infrasonic oscillations in the f2 region associated with severe thunderstorms. J. Geophys. Res. 86 (A7), 5873–5880. https://doi.org/10.1029/JA086iA07p05873.
Saito, A., Tsugawa, T., Otsuka, Y., et al., 2011. Acoustic resonance and plasma depletion detected by gps total electron content observation after the 2011 off the pacific coast of tohoku earthquake. Earth Planets Space 63 (7), 863–867. https://doi.org/10.5047/eps.2011.06.034.
Springer, T.A., 2000. Modeling and Validating Orbits and Clocks Using the Global Positioning System. Schweizerische Geodätische Kommission, Zürich, p. 60.
Tang, L., Chen, W., Chen, M., et al., 2019. Statistical observation of thunderstorm-induced ionospheric gravity waves above low-latitude areas in the northern hemisphere. Remote Sens. 11 (23). https://doi.org/10.3390/rs11232732, 2732(1–11).
Vadas, S.L., 2007. Horizontal and vertical propagation and dissipation of gravity waves in the thermosphere from lower atmospheric and thermospheric sources. J. Geophys. Res. 112 (A6), A06305. https://doi.org/10.1029/2006JA011845.
Vadas, S.L., Azeem, I., 2021. Concentric secondary gravity waves in the thermosphere and ionosphere over the continental united states on march 25–26, 2015 from deep convection. J. Geophys. Res.: Space Phys. 126 (2). https://doi.org/10.1029/2020JA028275, e2020JA028275.
Vadas, S.L., Fritts, D.C., 2004. Thermospheric responses to gravity waves arising from mesoscale convective complexes. J. Atmos. Sol. Terr. Phys. 66, 781–804. https://doi.org/10.1016/j.jastp.2004.01.025.
Vadas, S.L., Fritts, D.C., 2005. Thermospheric responses to gravity waves: Influences of increasing viscosity and thermal diffusivity. J. Geophys. Res. 110 (D15), D15103. https://doi.org/10.1029/2004JD005574.
Vadas, S.L., Liu, H.L., 2013. Numerical modeling of the large-scale neutral and plasma responses to the body forces created by the dissipation of gravity waves from 6 h of deep convection in brazil. J.

Geophys. Res. Space Phys. 118 (5), 2593–2617. https://doi.org/10.1002/jgra.50249.

Vadas, S.L., Liu, H.L., Lieberman, R.S., 2014. Numerical modeling of the global changes to the thermosphere and ionosphere from the dissipation of gravity waves from deep convection. J. Geophys. Res. Space Phys. 119, 7762–7793. https://doi.org/10.1002/2014JA020280.

Vadas, S.L., Xu, S., Yue, J., et al., 2019. Characteristics of the quiet-time hot spot gravity waves observed by goce over the southern andes on 5 July 2010. J. Geophys. Res.: Space Phys. 124 (8), 7034–7061. https://doi.org/10.1029/2019JA026693.

Vadas, S.L., Yue, J., She, C.-Y., et al., 2009. A model study of the effects of winds on concentric rings of gravity waves from a convective plume near fort collins on 11 May 2004. J. Geophys. Res. 114, D06103. https://doi.org/10.1029/2008JD010753.

Walterscheid, R.L., Schubert, G., Brinkman, D.G., 2003. Acoustic waves in the upper mesosphere and lower thermosphere generated by deep tropical convection. J. Geophys. Res. 108 (A11), 1392. https://doi.org/10.1029/2003JA010065.

Xiao, Z., Xiao, S., Hao, Y., et al., 2007. Morphological features of ionospheric response to typhoon. J. Geophys. Res. 112 (A4), A04304. https://doi.org/10.1029/2006JA011671.

Yue, J., Hoffmann, L., Alexander, M.J., 2013. Simultaneous observations of convective gravity waves from a ground-based airglow imager and the airs satellite experiment. J. Geophys. Res.: Atmos. 118 (8), 3178–3191. https://doi.org/10.1002/jgrd.50341.

Zettergren, M.D., Snively, J.B., 2013. Ionospheric signatures of acoustic waves generated by transient tropospheric forcing. Geophys. Res. Lett. 40 (20), 5345–5349. https://doi.org/10.1002/2013GL058018.